


RESEARCH

Open Access



# Neuroimaging-pathological correlations of [<sup>18</sup>F]THK5351 PET in progressive supranuclear palsy

Aiko Ishiki<sup>1</sup>, Ryuichi Harada<sup>1,2,9\*</sup> , Hideaki Kai<sup>3</sup>, Naomi Sato<sup>4</sup>, Tomoko Totsune<sup>5</sup>, Naoki Tomita<sup>1</sup>, Shoichi Watanuki<sup>6</sup>, Kotaro Hiraoka<sup>6</sup>, Yoichi Ishikawa<sup>6</sup>, Yoshihito Funaki<sup>6</sup>, Ren Iwata<sup>6</sup>, Shozo Furumoto<sup>6</sup>, Manabu Tashiro<sup>6</sup>, Hironobu Sasano<sup>4</sup>, Tetsuyuki Kitamoto<sup>3</sup>, Yukitsuka Kudo<sup>1</sup>, Kazuhiko Yanai<sup>2,6</sup>, Katsutoshi Furukawa<sup>7</sup>, Nobuyuki Okamura<sup>2,6,8</sup> and Hiroyuki Arai<sup>1</sup>

## Abstract

Recent positron emission tomography (PET) studies have demonstrated the accumulation of tau PET tracer in the affected region of progressive supranuclear palsy (PSP) cases. To confirm the binding target of radiotracer in PSP, we performed an imaging-pathology correlation study in two autopsy-confirmed PSP patients who underwent [<sup>18</sup>F]THK5351 PET before death. One patient with PSP Richardson syndrome showed elevated tracer retention in the globus pallidus and midbrain. In a patient with PSP-progressive nonfluent aphasia, [<sup>18</sup>F]THK5351 retention also was observed in the cortical areas, particularly the temporal cortex. Neuropathological examination confirmed PSP in both patients. Regional [<sup>18</sup>F]THK5351 standardized uptake value ratio (SUVR) in antemortem PET was significantly correlated with monoamine oxidase-B (MAO-B) level, reactive astrocytes density, and tau pathology at postmortem examination. In in vitro autoradiography, specific THK5351 binding was detected in the area of antemortem [<sup>18</sup>F]THK5351 retention, and binding was blocked completely by a reversible selective MAO-B inhibitor, lazabemide, in brain samples from these patients. In conclusion, [<sup>18</sup>F]THK5351 PET signals reflect MAO-B expressing reactive astrocytes, which may be associated with tau accumulation in PSP.

**Keywords:** PSP, Monoamine oxidase, Reactive astrocyte, Tau, PET, [<sup>18</sup>F]THK5351

## Introduction

Tau positron emission tomography (PET), which provides the topographic distribution of tau aggregates in the brain, would be useful for the diagnosis of Alzheimer's disease (AD) and for the assessment of tau burden in the clinical trials of antidementia drugs. Most studies on a tau PET radiopharmaceutical ([<sup>18</sup>F]AV1451) showed a robust difference between the control subjects and the patients with AD [16]. Regional distribution of [<sup>18</sup>F]AV1451 was correlated with tau neuropathology in *MAPT* R406W mutation carriers [37]. Tau PET also has

been considered potentially useful for antemortem assessment of non-AD tauopathies, such as progressive supranuclear palsy (PSP), corticobasal degeneration (CBD), and some variants of frontotemporal lobar degeneration (FTLD) [44]. [<sup>18</sup>F]AV1451 PET studies have shown elevated tracer retention where tau pathology was observed frequently in patients with PSP and CBD. However, several reports have highlighted the discrepancies between antemortem PET and postmortem in vitro binding studies, particularly in non-AD tauopathies. In vitro autoradiography validation studies demonstrated that [<sup>18</sup>F]AV1451 failed to bind to 4-repeat tau lesions in PSP and CBD [18, 24, 38]. Recent progress in the development of second-generation tau tracers successfully reduced the off-target binding in the basal ganglia and brainstem. However, to our knowledge, no tau PET radiopharmaceutical has been fully validated against neuropathology to date [23, 43]. [<sup>18</sup>F]THK5351 was one

\* Correspondence: [ryuichi.harada.c8@tohoku.ac.jp](mailto:ryuichi.harada.c8@tohoku.ac.jp)

<sup>1</sup>Department of Geriatrics and Gerontology, Division of Brain Science, Institute of Development, Aging and Cancer, Tohoku University, 4-1 Seiryomachi, Aoba-ku, Sendai, Miyagi, Japan

<sup>2</sup>Department of Pharmacology, Tohoku University School of Medicine, 2-1 Seiryomachi, Aoba-ku, Sendai, Miyagi, Japan

Full list of author information is available at the end of the article



of the first-generation tau PET radiotracers that was designed originally to detect tau aggregates in the form of PHF-tau in AD [11]. Clinical PET studies in PSP and CBS patients have demonstrated prominent [<sup>18</sup>F]THK5351 retention [2, 14, 19] in the midbrain and basal ganglia where tau pathology was observed frequently at autopsy [20, 45]. [<sup>18</sup>F]THK5351 binding in these areas is associated closely with disease progression because the amount of tracer retention was correlated positively with clinical severity of PSP [2]. However, recent studies have suggested the existence of off-target binding to monoamine oxidase-B (MAO-B). A single oral dose of selegiline, a selective irreversible MAO-B inhibitor, substantially reduced [<sup>18</sup>F]THK5351 binding in the brain of patients with PSP as well as AD [29]. In an autopsy case of AD, regional [<sup>18</sup>F]THK5351 binding was correlated significantly with MAO-B density as well as tau level. Therefore, [<sup>18</sup>F]THK5351 PET signal reflects the combination of tau pathology and reactive astrocytes in the AD brain [10]. However, what an [<sup>18</sup>F]THK5351 PET signal reflects in the PSP brain remains unclear.

We examined imaging-pathology correlation in two autopsy-confirmed PSP patients who showed prominent tracer retention on an antemortem [<sup>18</sup>F]THK5351 PET scan.

## Materials and methods

The ethics committee of the Tohoku University Graduate School of Medicine approved this study, and informed consent for neuroimaging and autopsy was obtained for each subject.

### PET and MRI scans and image analyses

PET images were acquired using an Eminence STARGATE PET scanner (Shimadzu, Kyoto, Japan). After intravenous injection of [<sup>18</sup>F]THK5351 (185 MBq) or [<sup>11</sup>C]PiB (296 MBq), dynamic PET images were obtained for 60 ([<sup>18</sup>F]THK5351) or 70 ([<sup>11</sup>C]PiB) minutes. T1-weighted magnetic resonance images (MRI) were obtained using a SIGNA 1.5-Tesla machine (General Electric, Milwaukee, WI, USA) according to a previously described method [14]. Standardized uptake value (SUV) images of [<sup>18</sup>F]THK5351 (40–60 min after injection) and [<sup>11</sup>C]PiB (50–70 min after injection) were obtained by normalizing tissue radioactivity concentration by injected dose and body weight. The regional SUV-to-cerebellar cortex SUV ratio (SUVR) was used as an index of tracer retention. SPM12 software (SPM12; Wellcome Department of Imaging Neuroscience, UCL, London, UK) was used to coregister the PET images on the MRI image. PMOD Ver. 3.7 software (PMOD Technologies GmbH, Zurich, Switzerland) was used to draw regions of interest (ROIs) on the coregistered MRI image.

### Brain tissue samples

The left hemisphere was immersed in 10% formalin for histology. The brain portions were frozen on powdered dry ice for biochemical analyses and unfixed tissue-based assays. Tissue sections of paraffin-embedded blocks were stained with Luixol fast blue and hematoxylin-eosin. Selected sections were stained with anti-tau AT8 (1:20; Innogenetics, Ghent, Belgium), anti- $\beta$ -amyloid 4G8 (1:10,000; BioLegend [Signet], San Diego, CA USA), anti- $\alpha$ -synuclein P-syn/81A (1:100, BioLegend [Covance]), anti-TDP43 pS409/410–1 (1:5000; Cosmo Bio, Tokyo, Japan), and anti-GFAP 6F2 (1:100; Agilent [Dako], Santa Clara, CA, USA) antibodies. Brain slices 12  $\mu$ m thick were generated with a cryostat (Microm HM560; Thermo Scientific, Waltham, MA, USA) using  $-20$  °C chamber and  $-15$  °C object temperatures. The sections were transferred to Matsunami Adhesive Slide (MAS)-coated glass slides (Matsunami Glass Ind., Ltd., Osaka, Japan). After drying, the sections were stored at  $-80$  °C. In subject 1, brain homogenates (0.1 mg/mL) additionally were prepared in phosphate-buffered saline (PBS) and stored at  $-80$  °C until experimental use.

### Quantification of tau and glial fibrillary acidic protein (GFAP) immunoreactivity

Microscopic images from each section of paraffin-embedded blocks were captured and a threshold of optical density was obtained by Image J software (National Institutes of Health [NIH], Bethesda, MD, USA). Tau and GFAP immunoreactivity was defined as total percentage of area covered by tau and GFAP immunostaining in each ROI.

### In vitro autoradiography of [<sup>18</sup>F]THK5351

The brain sections were dried and were dipped in PBS for a total of 25 min and, then, preincubated in PBS containing 1% bovine serum albumin (BSA). Then, the brain sections were incubated for 30 min at room temperature with [<sup>18</sup>F]THK5351 (370 kBq/mL). After incubation, the sections were washed sequentially with PBS containing 1% BSA for 5 min, followed by PBS for 5 min twice. The dried sections were exposed to an imaging plate (BAS IP MS 2025 E; GE Healthcare, Little Chalfont, UK) overnight. Autoradiographic images were obtained from Typhoon FLA-9500 (GE Healthcare). To account for the binding to MAO-B in brain tissues, the reaction was incubated in the presence of MAO-B inhibitor, Lazabemide (1  $\mu$ M). After post-fixation in 4% paraformaldehyde for 30 min, adjacent frozen sections were immunostained with anti-tau AT8, anti-MAO-B (1:400, Sigma-Aldrich Corp., St. Louis, MO, USA), and anti-GFAP 6F2 antibodies.

### In vitro binding assay of [<sup>3</sup>H]THK5351

The reaction mixture contained [<sup>3</sup>H]THK5351 (1 nM; specific activity, 2.96 TBq/mmol; radiochemical purity, 98.9%; Sekisui Medical, Inc., Tokyo, Japan) and brain homogenates (0.5 μg), in a final volume 200 μL. Nonspecific binding was defined in the presence of 2 μM unlabeled THK5351. The mixture was incubated at room temperature for 2 h, and separation of bound from free radioactivity was achieved by filtration under reduced pressure (Multiscreen HTS Vacuum Manifold, Multiscreen HTS 96-well 0.65 μm filtration plate; Millipore, Billerica, MA, USA), followed by three washes with PBS containing 0.1% BSA. The filters were incubated in 2 mL scintillation fluid (Emulsifier-Safe; Perkin Elmer, Boston, MA, USA), and a β counter (LS6500 liquid scintillation counter; Beckman Coulter, Brea, CA, USA) was used to count the radioactivity.

### Semiquantification of PHF-tau by immunoblotting

Immunoblotting for PHF-tau was performed according to a previously reported protocol [39]. After centrifugation (20,000 g, 15 min, 4 °C) of brain homogenates, the resulting pellet was dissolved in extraction buffer containing 10 mM Tris-HCl (pH 7.5), 0.8 M NaCl, 10% sucrose, 1 mM ethylene glycol-bis β-aminoethyl ether (EGTA), 2% sarkosyl, and then incubated for 30 min at 37 °C. The supernatants were collected after centrifugation at 20,000 g for 10 min at 25 °C. After ultracentrifugation (100,000 g, 20 min, 25 °C), the pellets were washed with 0.5 mL sterile saline and solubilized in sodium dodecyl sulfate (SDS)-sample buffer and, then, run on a 5–20% gradient polyacrylamide gel (SuperSep™ Ace; Wako, Osaka, Japan). Proteins were transferred to polyvinylidene fluoride (PVDF) membrane, blocked by incubation with 3% gelatin (Wako) for 10 min at 37 °C, followed by overnight incubation at room temperature with the anti-tau monoclonal antibody T46 (1:2000, Thermo Fisher Scientific), biotinylated anti-mouse secondary antibody, ABC complex (Vector Laboratories, Burlingame, CA, USA) and developed with diaminobenzidine and nickel chloride. For semiquantification of sarkosyl-insoluble tau, the three dominant bands (68, 64, and 60 kDa) were quantified by ImageJ software (Additional file 1: Figure S1). Sarkosyl-insoluble tau (PHF-tau) was expressed as ratio using cerebellum as reference.

### Quantification of MAO-B and GFAP by enzyme-linked immunosorbent assay (ELISA)

Brain MAO-B levels were quantified using a human MAO-B ELISA kit (Ab157393, Abcam, Cambridge, UK) with MAO-B standard (M7441, Sigma-Aldrich Corp.). Extraction of MAO-B was performed according to the manufacturer's instructions. For the quantification of

GFAP, brain homogenates were extracted with Tris-HCl buffer containing 0.1% Triton-X as described previously [13]. A human GFAP ELISA kit (BioVendor, Asheville, NC, USA) was used to quantify the GFAP levels.

### Statistical analysis

Spearman rank correlation coefficients were calculated to examine the association between radiotracer binding, histopathology, and biochemical data. Statistical significance was defined at  $P < 0.05$ . GraphPad Prism software (GraphPad, San Diego, CA, USA) was used to perform this analysis.

## Results

### Case reports

#### Subject 1

An 84-year-old right-handed male presented with memory disturbance and disorientation. One year later, standing and gait became unstable with progression of extrapyramidal signs and PSP was diagnosed clinically. PET scans were performed 2 years after the diagnosis of PSP. At the time of the PET scan, he was bedridden and the Mini-Mental State Examination (MMSE) score was 1 of 30. Neurologic examinations revealed limited vertical eye movement. The PSP rating scale score was 82. A brain MRI showed significant midbrain atrophy. A typical “hummingbird sign” was observed in the sagittal section. He died of aspiration pneumonia 295 days after the PET scan. Detailed clinical information has been described previously [14].

#### Subject 2

A 73-year-old right-handed male presented with memory disturbance. Mild cognitive impairment was diagnosed clinically 3 years after the first symptoms appeared. He gradually presented with speech impairment, stereotypical behavior, and change of food preference, and progressive nonfluent aphasia (PNFA) was diagnosed. We did not perform DNA sequencing to confirm a mutation in the *MAPT* gene. One year later, he presented with unstable gait and was prone to falls. At the PET scan, he was bedridden and the MMSE score was 1 of 30. An MRI showed diffuse brain atrophy prominent in the right anterior temporal, hippocampus, amygdala, and caudate nuclei. He died of aspiration pneumonia 79 days after PET scan.

### [<sup>18</sup>F]THK5351 and [<sup>11</sup>C]PiB PET scans

Figure 1 shows the [<sup>18</sup>F]THK5351 PET images from the two subjects. Images from a cognitively normal individual are shown for comparison at the bottom (Fig. 1). Subject 1 showed significant [<sup>18</sup>F]THK5351 retention in the globus pallidus and midbrain. Mild tracer retention was observed also in the other cortices, including

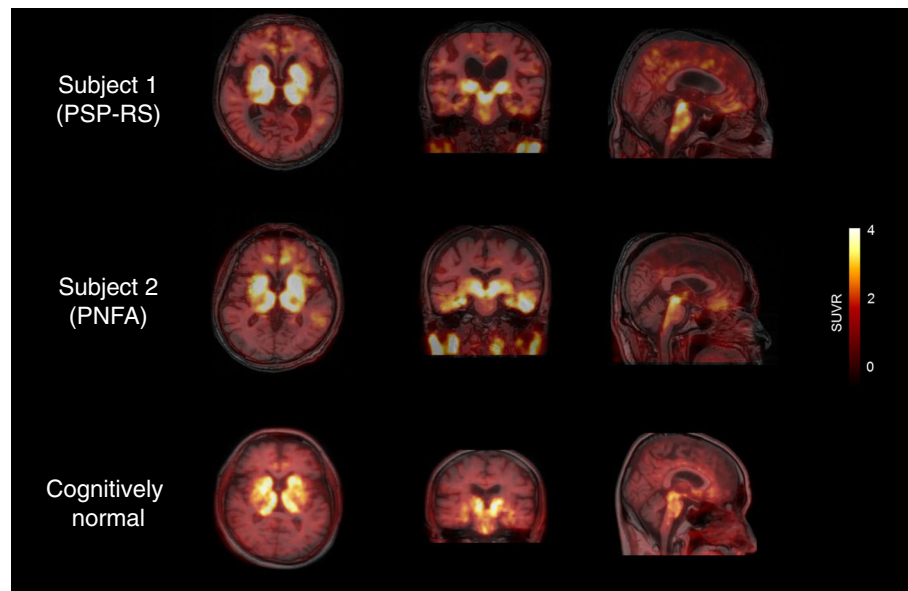


**Fig. 1** [ $^{18}\text{F}$ ]THK5351 PET images from two study subjects and a cognitively normal subject. The scale indicates SUVR range from 0 to 4

parahippocampal and inferior temporal gyri. Subject 2 showed prominent [ $^{18}\text{F}$ ]THK5351 retention in the parahippocampal and inferior temporal gyri, as well as the globus pallidus and midbrain. No remarkable retention of [ $^{11}\text{C}$ ]PiB was observed in the neocortex in both of the subjects (data not shown).

#### Neuropathological examination

Brain weight in subject 1 was 1580 g. Autopsy revealed severe atrophy in the midbrain tegmentum and pons, and subthalamic nucleus, and relatively mild atrophy in the frontal cortex, but not in the basal ganglia. Neuropathological examination revealed tau pathology in neuronal and glial cells consistent with PSP. Globose tangles were observed in the midbrain, pons, medulla, subthalamic nucleus, and nucleus basalis of Meynert. Moderate numbers of tufted astrocytes were observed also in the amygdala, motor cortex, and superior frontal gyrus. Neurofibrillary tangles were observed in the entorhinal cortex and subiculum, which corresponded to age-related Braak stage II [1]. The tau immunoreactivity density appeared greatest in the medial temporal regions, followed by the basal ganglia and frontal cortex. Small cerebral infarctions were observed in the putamen and the cerebellum. Gliosis and neuronal loss were observed also in the substantia nigra. However, amyloid- $\beta$ ,  $\alpha$ -synuclein, and TDP-43 pathology were absent in this case. These characteristics were consistent with the diagnosis of definite PSP.

Brain weight in subject 2 was 920 g. Autopsy revealed severe atrophy in bilateral temporal lobes, including the hippocampus and amygdala. Brain atrophy was

obviously observed in the tegmentum of the midbrain and pons. There was neuronal loss in the pigmented neurons of the substantia nigra and locus coeruleus. Brain atrophy was observed also in the globus pallidus, hypothalamic nucleus, and cerebellar dentate nucleus. AT8 immunostaining revealed abundant tau burden, including neurofibrillary tangles, globose tangles, tufted astrocytes, coiled bodies, and neuropil threads in the temporal, cingulate, frontal, striatum, globus pallidus, and subthalamic nucleus. In addition, thorn-shaped astrocytes, typical in aging-related tau astrogliaopathy, were observed in the temporal lobe gray and white matter [21]. Sparse amyloid plaques were observed in the cerebral cortex (Thal phase for A $\beta$  plaques: 2, CERAD: Sparse). Both  $\alpha$ -synuclein and TDP-43 pathology were absent in this case. Gliosis was severe in the bilateral hippocampus and amygdala. Astrocytosis with neuronal loss was prominent in the temporal cortex, followed by the frontal and cingulate cortices. Three- and four-repeat tau-immunohistochemistry studies, respectively, revealed that these tau lesions were composed of four-repeat tau. The distribution, isoform, and morphology of tau immunoreactive lesions were consistent with atypical PSP [17], which was diagnosed as PSP-FTD.

#### In vivo–in vitro correlation analyses

Biochemical analysis revealed the presence of sarkosyl-insoluble tau (68 and 64 kDa), corresponding to 4-repeat tau protein in both cases (Additional file 1: Figure S1). In subject 1, sarkosyl-insoluble tau was high in the parahippocampal gyrus and hippocampus,

moderate in the globus pallidus and putamen, and low in other areas (Fig. 2a). The parahippocampal gyrus contained 3- (60 kDa band) and 4-repeat tau, suggesting that they are age-related tau. AT8 immunohistochemistry was positive in the brain sections from the same tissue (data not shown). In subject 1, in vivo [ $^{18}\text{F}$ ]THK5351 binding was correlated significantly with sarkosyl-insoluble tau levels determined by Western blot analysis ( $r = 0.67$ ,  $P = 0.039$ ; Fig. 2b). In addition, we found a strong correlation between in vivo [ $^{18}\text{F}$ ]THK5351 binding and MAO-B levels ( $r = 0.78$ ,  $P = 0.0096$ ; Fig. 2c). A significant positive correlation was observed also between in vivo [ $^{18}\text{F}$ ]THK5351 binding and GFAP level ( $r = 0.67$ ,  $P = 0.039$ ; Fig. 2d). In vitro [ $^3\text{H}$ ]THK5351 binding assay using brain homogenates also demonstrated a strong correlation between in vivo [ $^{18}\text{F}$ ]THK5351 retention and in vitro tracer binding in subject 1 ( $r = 0.92$ ,  $P = 0.005$ ; Fig. 2e). Tau and GFAP immunoreactivities in the brain sections were measured quantitatively for correlation analysis between in vivo tracer retention and histopathology (Fig. 3). We observed positive correlation trends between in vivo [ $^{18}\text{F}$ ]THK5351 retention and tau loads ( $r = 0.48$ ,  $P = 0.06$ ), and between in vivo [ $^{18}\text{F}$ ]THK5351 retention and GFAP immunoreactivity ( $r = 0.49$ ,  $P = 0.05$ ).

In subject 2, in vivo [ $^{18}\text{F}$ ]THK5351 binding was correlated significantly with tau-immunohistochemistry

using AT8 antibody ( $r = 0.48$ ,  $P = 0.037$ ; Fig. 4b). Furthermore, in vivo [ $^{18}\text{F}$ ]THK5351 retention was correlated positively with the density of GFAP immunoreactive astrocytes ( $r = 0.64$ ,  $P = 0.0033$ ).

#### In vitro autoradiography

In vitro autoradiography of [ $^{18}\text{F}$ ]THK5351 in frozen sections demonstrated high tracer binding in the globus pallidus as well as putamen in subject 1 and in the frontal cortex in subject 2 (Fig. 5), which was consistent with in vivo PET results (Fig. 1). These bindings were displaced completely after treatment with MAO-B inhibitor, Lazabemide [10]. The spatial pattern of [ $^{18}\text{F}$ ]THK5351 binding was similar to that of MAO-B immunostaining, suggesting that the target of [ $^{18}\text{F}$ ]THK5351 binding was MAO-B-positive astroglia rather than the tau aggregates in the PSP brain.

#### Discussion

Tremendous efforts have been made to develop tau-selective PET radiopharmaceuticals. The first-generation tau PET tracers, such as [ $^{11}\text{C}$ ]PBB3, [ $^{18}\text{F}$ ]AV1451, and [ $^{18}\text{F}$ ]THK5351, have shown accumulation in the predilection site for tau deposition. Tau PET imaging recapitulated topographical regional distribution patterns similar to those reported by Braak staging of tau pathology at autopsy [44]. However, they showed nonnegligible off-target

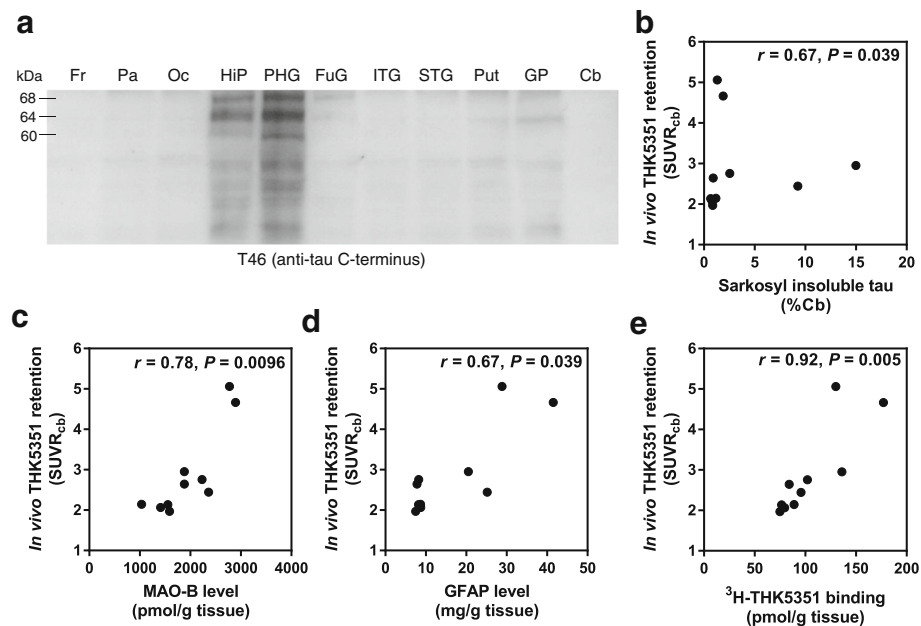
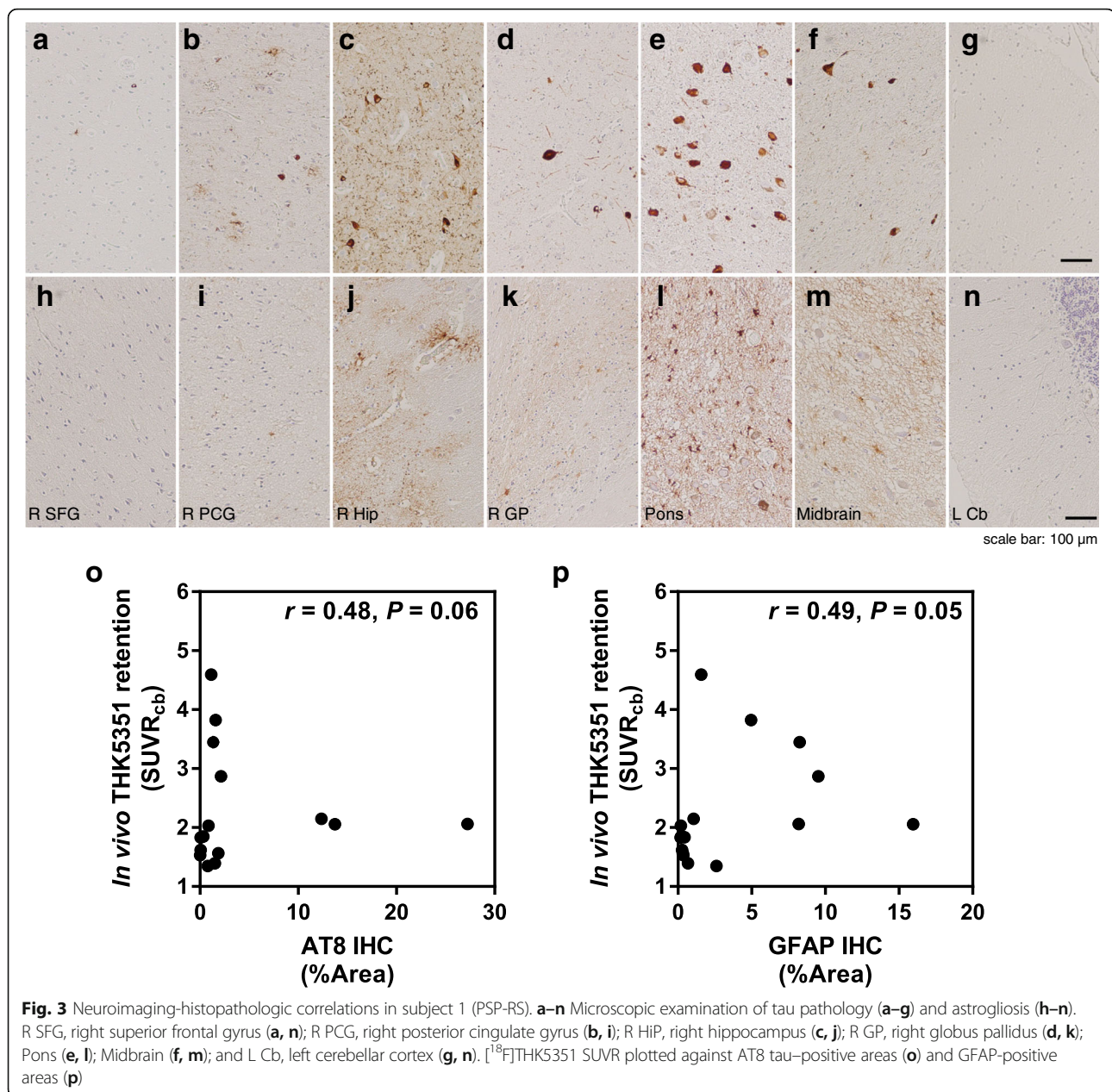


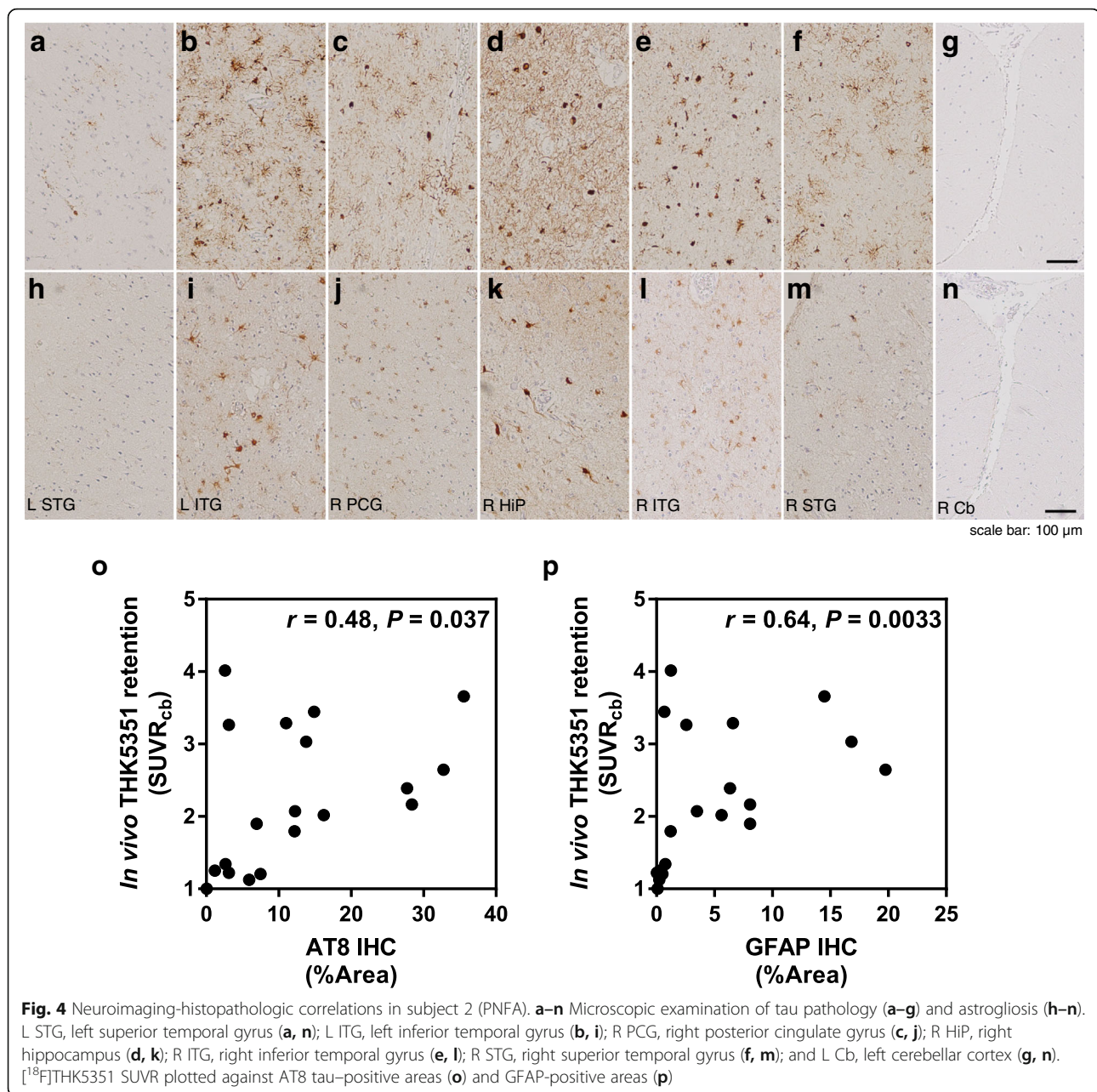
**Fig. 2** Neuroimaging, biochemical, in vitro binding correlations in subject 1 (PSP-RS). **a** Immunoblot analysis of sarkosyl-insoluble tau; 11 regions (Fr, frontal cortex; Pa, parietal cortex; Oc, occipital cortex; HiP, hippocampus; PHG, parahippocampal gyrus; FuG, fusiform gyrus; ITG, inferior temporal gyrus; STG, superior temporal gyrus; Put, putamen; GP, globus pallidus; Cb, Cerebellum) detected by T46 (anti-tau C-terminus). **b** [ $^{18}\text{F}$ ]THK5351 SUVr plotted against sarkosyl-insoluble tau level (%cerebellum). **c** [ $^{18}\text{F}$ ]THK5351 SUVr plotted against MAO-B level. **d** [ $^{18}\text{F}$ ]THK5351 SUVr plotted against GFAP level. **e** [ $^{18}\text{F}$ ]THK5351 SUVr plotted against in vitro [ $^3\text{H}$ ]THK5351 binding



binding [4, 11, 27]. A recent human blocking study using selegiline demonstrated binding of [<sup>18</sup>F]THK5351 to MAO-B [29]. Furthermore, the regional [<sup>18</sup>F]THK5351 binding was correlated significantly with density of MAO-B in our autopsy case of AD [10]. In this study, we expanded the imaging-pathology correlation analysis to autopsy-confirmed PSP cases showing two different clinical phenotypes, Richardson syndrome (PSP-RS) and PNFA.

A patient with PSP-RS showed remarkable [<sup>18</sup>F]THK5351 retention in the globus pallidus and midbrain [2, 14]. The spatial distribution of [<sup>18</sup>F]THK5351 retention in this patient was similar to the topographical

distribution of tau pathology in cases of classic PSP-RS [45]. Postmortem examination of this patient confirmed the existence of 4-repeat tau aggregates in these regions. However, imaging-pathology correlation analysis indicated a significant correlation between *in vivo* [<sup>18</sup>F]THK5351 retention and MAO-B level. Furthermore, *in vitro* autoradiography demonstrated that [<sup>18</sup>F]THK5351 binding in the globus pallidus was displaced by the MAO-B inhibitor, suggesting that [<sup>18</sup>F]THK5351 mainly binds to the MAO-B rather than the 4-repeat tau aggregates. In our previous study using paraffin-embedded fixed brain sections, we observed specific binding of [<sup>18</sup>F]THK5351 to tufted astrocytes



and neurofibrillary tangles in the PSP brain [14]. However, the fixation of tissues and use of alcohol in the differentiation process may affect the tracer binding (i.e., diminishing the natural binding sites and/or yielding artificial binding sites) in in vitro autoradiography experiments. In this study, we performed in vitro autoradiographs of fresh-frozen sections without using alcohol and found a substantial amount of tracer binding to MAO-B. Fresh-frozen section results showed good agreement with antemortem [<sup>18</sup>F]THK5351 PET analysis. These results highlighted the importance of appropriate experimental procedures in the validation of PET radiopharmaceuticals.

[<sup>18</sup>F]AV1451 PET studies in PSP cases have shown high tracer retention in the globus pallidus and mid-brain, as observed in [<sup>18</sup>F]THK5351 PET. However, the postmortem in vitro autoradiography did not show any significant binding of [<sup>18</sup>F]AV1451 in these brain regions [18, 24, 38]. The discrepancy between in vitro and in vivo PET results may be explained also by the same technical problems as those observed in THK5351. Most of these studies used high concentrations of ethanol in the differentiation process of autoradiography [5, 25, 33, 46]. High binding affinity of [<sup>18</sup>F]AV1451 to monoamine oxidases (MAO-A and MAO-B for  $K_d=1.6$  nM and 21 nM, respectively) was observed in in vitro binding

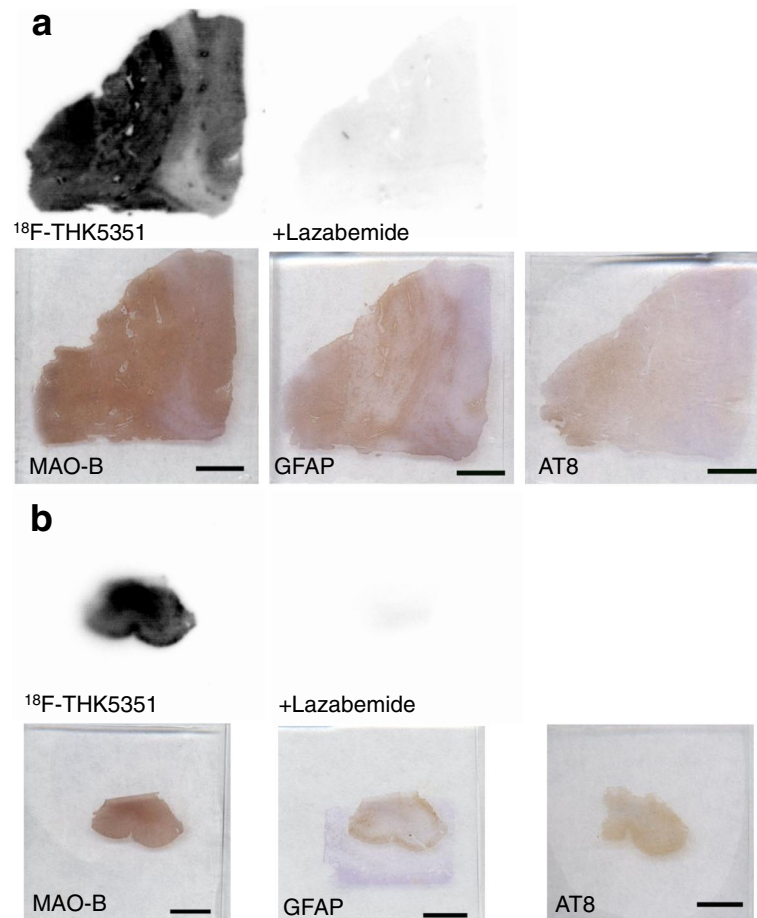


**Fig. 5** In vitro autoradiography of [ $^{18}\text{F}$ ]THK5351 and immunohistochemistry (MAO-B, GFAP, AT8-tau) in frozen sections from subjects. **a** Basal ganglia from subject 1 and **b** frontal cortex from subject 2. The specific binding to MAO-B was confirmed by a reversible MAO-B inhibitor, Lazabemide. Scale bars: 5 mm

assay [42]. [ $^{18}\text{F}$ ]AV1451 binding to MAO may be overlooked by the use of ethanol. Retrospective investigation of [ $^{18}\text{F}$ ]AV1451 PET in patients with Parkinson's disease showed no significant difference between conditions before and after treatment with irreversible MAO-B inhibitors (selegiline and rasagiline) [9]. Therefore, the dominant off-target binding substrates of [ $^{18}\text{F}$ ]AV1451 would be MAO-A or other unknown molecules.

We observed a significant correlation between tau pathology and GFAP in both of our subjects. Tau pathology in PSP includes neurofibrillary tangles, tufted astrocytes, coiled bodies, and threads pathology [45]. A postmortem study reported that the density of GFAP correlated with that of neurofibrillary tangles, but not with tufted astrocytes in PSP, suggesting the greater contribution of neurofibrillary tangles to astrogliosis in PSP [40]. MAO-B is expressed dominantly in the mitochondrial outer membrane of astrocytes. Since elevation of MAO-B levels in the brain has been implicated in several neurodegenerative diseases, MAO-B is an attractive

target as a molecular imaging marker of astrogliosis [7]. Recently, a postmortem study in parkinsonian conditions, including PSP, demonstrated that MAO-B levels elevated remarkably in the midbrain of PSP and positively correlated with astroglial markers, such as GFAP, vimentin, and Hsp27 [41], which was consistent with our observation. MAO-B PET imaging using [ $^{11}\text{C}$ ]L-deprenyl-D2 showed elevated tracer retention in the brain of several neurodegenerative diseases including AD [6, 15, 34]. Other investigators have reported the elevation of tracer binding in prodromal AD, but not in symptomatic AD [3, 30, 36]. However, many postmortem studies have shown the elevation of MAO-B levels in the postmortem brains of AD [8, 26, 35]. As discussed previously [41], this discrepancy might be explained by the low sensitivity of [ $^{11}\text{C}$ ]L-deprenyl-D2 PET. Recently, second-generation MAO-B PET tracers, such as [ $^{11}\text{C}$ ]SL25.1188, have been developed and showed reversible binding to MAO-B [31, 32]. Furthermore, the development of [ $^{18}\text{F}$ ]labeled PET tracers is ongoing [12, 28].



Our study strongly supported that [<sup>18</sup>F]THK5351 PET dominantly reflected the binding to MAO-B in patients with PSP. Therefore, [<sup>18</sup>F]THK5351 PET would be useful for in vivo assessment of astrogliosis in PSP. Future research should proceed with development of PET tracers for selective detection of astrogliosis and sensitive detection of 4-repeat tau in the human brain. -

In PSP-RS cases, ischemic changes observed in the putamen might induce reactive astrocytes. Recently, reactive astrocytes have been categorized into two different types depending on the gene expression: A1 astrocytes highly upregulated many classical complement cascades and are toxic as observed in neuroinflammation; A2 astrocytes upregulated many neurotrophic factors and are protective as observed in ischemia [22]. The GFAP showed elevated expression in both reactive astrocytes. [<sup>18</sup>F]THK5351 PET signal in the putamen of PSP-RS cases may reflect elevation of MAO-B levels induced by ischemia. Further studies are required to clarify MAO-B expression profiles in reactive astrocytes subtypes.

## Conclusions

Our imaging-pathology validation study demonstrated the binding of [<sup>18</sup>F]THK5351 to MAO-B-positive astrogliosis in the PSP brain. Therefore, [<sup>18</sup>F]THK5351 PET may be useful to assess astrocytosis in non-AD tauopathies.

## Additional file

**Additional file 1: Figure S1.** Immunoblot analysis of sarkosyl-insoluble tau in the study subject and an AD case detected by T46 (anti-tau C-terminus). The study subjects contained dominantly 4R tau (64- and 68-kDa tau). (PPTX 334 kb)

## Abbreviations

3R: 3 repeat; 4R: 4 repeat; AD: Alzheimer's disease; BSA: Bovine serum albumin; Cb: Cerebellum; CBD: Corticobasal degeneration; CBS: Corticobasal syndrome; ELISA: Enzyme-linked immunosorbent assay; Fr: Frontal cortex; FTLD: Frontotemporal lobar degeneration; FuG: Fusiform gyrus; GFAP: Glial fibrillar acid protein; GP: Globus pallidus; Hip: Hippocampus; ITG: Inferior temporal gyrus; L Cb: Left cerebellar cortex; MAO-B: Monoamine oxidase-B; MRI: Magnetic resonance imaging; Oc: Occipital cortex; Pa: Parietal cortex; PBS: Phosphate-buffered saline; PET: Positron emission tomography; PHF: Paired helical filament; PHG: Parahippocampal gyrus; PNFA: Progressive nonfluent aphasia; PSP: Progressive supranuclear palsy; PSP-RS: Progressive supranuclear palsy Richardson syndrome; Put: Putamen; R GP: Right globus pallidus; R PCG: Right posterior cingulate gyrus; R SFG: Right superior frontal gyrus; STG: Superior temporal gyrus; SUV: Standardized uptake value; SUVr: Standardized uptake value ratio

## Acknowledgements

We are grateful to the study subjects and the staffs for Cyclotron and Radioisotope Center, Tohoku University.

## Funding

This study was supported by research funds from GE Healthcare, the SEI (Sumitomo Electric Industries, Ltd.) Group CSR Foundation, Grant-in-Aid for Research Activity Start-up (16H06621), Grant-in-Aid for Young Scientists (B) (15 K19767), Grant-in-Aid for Scientific Research (B) (15H04900), Grant-in-Aid for Scientific Research on Innovative Areas (Brain Protein Aging and

Dementia Control) (26117003) from MEXT and Shimazu Science Foundation. This work is partially supported by the Initiative for Realizing Diversity in the Research Environment (Tohoku University Morinomiya Project for Empowering Women in Research) from Japan Science and Technology Agency, JST.

## Availability of data and materials

The datasets used and analysed during the current study available from the corresponding author on reasonable request.

## Authors' contributions

AI, RH, KF, and NO conceived the study and participated in its design and coordination. AI, SW, KH, MT, and NO acquired PET images. AI, TT, NT, KF, and AH performed clinical examination. AI and NO carried out PET image analysis. RH carried out biochemical analysis, immunostaining, and autoradiography. AI, RH, and NO carried out neuroimaging-pathological correlations and performed statistical analysis and drafted the manuscript. YI, YF, SF, and RI carried out radiosynthesis. HK, NS, HS, and TK carried out autopsy, preparing tissues, immunostaining, and neuropathologic examination. YK, KY, KF, and HA supervised the study. All the authors read and approved the final manuscript.

## Ethics approval and consent to participate

All the procedures performed in studies involving human participants were in accordance with the ethical standards of the institutional committee and with the 1964 Helsinki Declaration and its later amendments.

## Consent for publication

Informed consent was obtained from all the individual participants included in the study and according to the institutional procedures for autopsy consents for postmortem tissue.

## Competing interests

NO, SF, and YK received the research funding from GE Healthcare. NO and YK own stock of CLINO Ltd.

## Publisher's Note

Springer Nature remains neutral with regard to jurisdictional claims in published maps and institutional affiliations.

## Author details

<sup>1</sup>Department of Geriatrics and Gerontology, Division of Brain Science, Institute of Development, Aging and Cancer, Tohoku University, 4-1 Seiryomachi, Aoba-ku, Sendai, Miyagi, Japan. <sup>2</sup>Department of Pharmacology, Tohoku University School of Medicine, 2-1 Seiryomachi, Aoba-ku, Sendai, Miyagi, Japan. <sup>3</sup>Department of Neurological Science, Tohoku University School of Medicine, 2-1 Seiryomachi, Aoba-ku, Sendai, Miyagi, Japan. <sup>4</sup>Department of Pathology, Tohoku University School of Medicine, 4-1 Seiryomachi, Aoba-ku, Sendai, Miyagi, Japan. <sup>5</sup>Department of Nuclear Medicine and Radiology, Institute of Development, Aging and Cancer, Tohoku University, 4-1 Seiryomachi, Aoba-ku, Sendai, Miyagi, Japan. <sup>6</sup>Cyclotron and Radioisotope Center, Tohoku University, 6-3 Aoba, Aramaki, Aoba-ku, Sendai, Miyagi, Japan. <sup>7</sup>Division of Community Medicine, Faculty of Medicine, Tohoku Medical and Pharmaceutical University, 1-15-1 Fukumuro, Miyagino-ku, Sendai, Miyagi, Japan. <sup>8</sup>Division of Pharmacology, Faculty of Medicine, Tohoku Medical and Pharmaceutical University, 1-15-1 Fukumuro, Miyagino-ku, Sendai, Miyagi, Japan. <sup>9</sup>Department of Pharmacology, Tohoku University School of Medicine 2-1, Seiryomachi, Aoba-ku, Sendai 9808575, Japan.

Received: 12 June 2018 Accepted: 19 June 2018

Published online: 29 June 2018

## References

- Braak H, Alafuzoff I, Arzberger T, Kretschmar H, Del Tredici K (2006) Staging of Alzheimer disease-associated neurofibrillary pathology using paraffin sections and immunocytochemistry. *Acta Neuropathol* 112:389–404
- Brendel M, Schonecker S, Hoglinger G, Lindner S, Havla J, Blautzik J et al (2017) [<sup>18</sup>F]-THK5351 PET correlates with topology and symptom severity in progressive supranuclear palsy. *Front Aging Neurosci* 9:440
- Carter SF, Scholl M, Almkvist O, Wall A, Engler H, Langstrom B et al (2012) Evidence for astrocytosis in prodromal Alzheimer disease provided by <sup>11</sup>C-

- deuterium-L-deprenyl: a multitracer PET paradigm combining  $^{11}\text{C}$ -Pittsburgh compound B and  $^{18}\text{F}$ -FDG. *J Nucl Med* 53:37–46
4. Chien DT, Bahri S, Szardenings AK, Walsh JC, Mu F, Su MY et al (2013) Early clinical PET imaging results with the novel PHF-tau radioligand [F-18]-T807. *J Alzheimers Dis* 34:457–468
  5. Declercq L, Celen S, Lecina J, Ahamed M, Tousseyn T, Moechars D et al (2016) Comparison of new tau PET-tracer candidates with [ $^{18}\text{F}$ ]T808 and [ $^{18}\text{F}$ ]T807. *Mol Imaging* 15:1–15
  6. Engler H, Nennesmo I, Kumlien E, Gambini JP, Lundberg P, Savitcheva I et al (2012) Imaging astrocytosis with PET in Creutzfeldt-Jakob disease: case report with histopathological findings. *Int J Clin Exp Med* 5:201–207
  7. Fowler JS, Logan J, Shumay E, Alia-Klein N, Wang GJ, Volkow ND (2015) Monoamine oxidase: radiotracer chemistry and human studies. *J Labelled Comp Radiopharm* 58:51–64
  8. Gulyas B, Pavlova E, Kasa P, Gulya K, Bakota L, Varszegi S et al (2011) Activated MAO-B in the brain of Alzheimer patients, demonstrated by [ $^{11}\text{C}$ ]-L-deprenyl using whole hemisphere autoradiography. *Neurochem Int* 58:60–68
  9. Hansen AK, Brooks DJ, Borghammer P (2018) MAO-B inhibitors do not block in vivo flortaucipir[ $^{18}\text{F}$ ]-AV-1451 binding. *Mol Imaging Biol* 20:356–360
  10. Harada R, Ishiki A, Kai H, Sato N, Furukawa K, Furumoto S et al (2017) Correlations of  $^{18}\text{F}$ -THK5351 PET with post-mortem burden of tau and astrogliosis in Alzheimer's disease. *J Nucl Med* 59:671–674
  11. Harada R, Okamura N, Furumoto S, Furukawa K, Ishiki A, Tomita N et al (2016)  $^{18}\text{F}$ -THK5351: a novel PET radiotracer for imaging neurofibrillary pathology in Alzheimer disease. *J Nucl Med* 57:208–214
  12. Hicks JW, Sadvovsk O, Parkes J, Houle S, Hay BA, Carter RL et al (2015) Radiosynthesis and ex vivo evaluation of [ $^{18}\text{F}$ ]-5-(3-(6-(3-fluoropropoxy)benzo[d]isoxazol-3-yl)-5-(methoxymethyl)oxazoli) din-2-one for imaging MAO-B with PET. *Bioorg Med Chem Lett* 25:288–291
  13. Ingelsson M, Fukumoto H, Newell KL, Growdon JH, Hedley-Whyte ET, Frosch MP (2004) Early Abeta accumulation and progressive synaptic loss, gliosis, and tangle formation in AD brain. *Neurology* 62:925–931
  14. Ishiki A, Harada R, Okamura N, Tomita N, Rowe CC, Villemagne VL et al (2017) Tau imaging with [ $^{18}\text{F}$ ]THK-5351 in progressive supranuclear palsy. *Eur J Neurol* 24:130–136
  15. Johansson A, Engler H, Blomquist G, Scott B, Wall A, Aquilonius SM et al (2007) Evidence for astrocytosis in ALS demonstrated by [ $^{11}\text{C}$ ](L)-deprenyl-D2 PET. *J Neurol Sci* 255:17–22
  16. Johnson KA, Schultz A, Betensky RA, Becker JA, Sepulcre J, Rentz D et al (2016) Tau positron emission tomographic imaging in aging and early Alzheimer disease. *Ann Neurol* 79:110–119
  17. Josephs KA, Boeve BF, Duffy JR, Smith GE, Knopman DS, Parisi JE et al (2005) Atypical progressive supranuclear palsy underlying progressive apraxia of speech and nonfluent aphasia. *Neurocase* 11:283–296
  18. Josephs KA, Whitwell JL, Tacik P, Duffy JR, Senjem ML, Tosakulwong N et al (2017) [ $^{18}\text{F}$ ]AV-1451 tau-PET uptake does correlate with quantitatively measured 4R-tau burden in autopsy-confirmed corticobasal degeneration. *Acta Neuropathol* 132:931–933
  19. Kikuchi A, Okamura N, Hasegawa T, Harada R, Watanuki S, Funaki Y et al (2016) In vivo visualization of tau deposits in corticobasal syndrome by  $^{18}\text{F}$ -THK5351 PET. *Neurology* 87:2309–2316
  20. Kouri N, Murray ME, Hassan A, Rademakers R, Uitti RJ, Boeve BF et al (2017) Neuropathological features of corticobasal degeneration presenting as corticobasal syndrome or Richardson syndrome. *Brain* 134:3264–3275
  21. Kovacs GG, Ferrer I, Grinberg LT, Alafuzoff I, Attems J, Budka H et al (2016) Aging-related tau astrogliopathy (ARTAG): harmonized evaluation strategy. *Acta Neuropathol* 131:87–102
  22. Liddelov SA, Guttenplan KA, Clarke LE, Bennett FC, Bohlen CJ, Schirmer L et al (2017) Neurotoxic reactive astrocytes are induced by activated microglia. *Nature* 541:481–487
  23. Lois C, Gonzalez I, Johnson KA, Price JC (2018) PET imaging of tau protein targets: a methodological perspective. *Brain Imaging Behav* 1:1–2
  24. Marquie M, Normandin MD, Meltzer AC, Siao Tick Chong M, Andrea NV, Anton-Fernandez A et al (2017) Pathological correlations of [F-18]-AV-1451 imaging in non-alzheimer tauopathies. *Ann Neurol* 81:117–128
  25. Marquie M, Normandin MD, Vanderburg CR, Costantino IM, Bien EA, Rycyna LG et al (2015) Validating novel tau positron emission tomography tracer [F-18]-AV-1451 (T807) on postmortem brain tissue. *Ann Neurol* 78:787–800
  26. Marutle A, Gillberg PG, Bergfors A, Yu W, Ni R, Nennesmo I et al (2013)  $^3\text{H}$ -deprenyl and  $^3\text{H}$ -PIB autoradiography show different laminar distributions of astroglia and fibrillar beta-amyloid in Alzheimer brain. *J Neuroinflammation* 10:90
  27. Maruyama M, Shimada H, Suhara T, Shinotoh H, Ji B, Maeda J et al (2013) Imaging of tau pathology in a tauopathy mouse model and in Alzheimer patients compared to normal controls. *Neuron* 79:1094–1108
  28. Nag S, Fazio P, Lehmann L, Ketschou G, Heinrich T, Thiele A et al (2016) In vivo and in vitro characterization of a novel MAO-B inhibitor Radioligand,  $^{18}\text{F}$ -labeled deuterated Fluorodeprenyl. *J Nucl Med* 57:315–320
  29. Ng KP, Pascoal TA, Mathotaarachchi S, Therriault J, Kang MS, Shin M et al (2017) Monoamine oxidase B inhibitor, selegiline, reduces  $^{18}\text{F}$ -THK5351 uptake in the human brain. *Alzheimers Res Ther* 9:25
  30. Rodriguez-Vieitez E, Saint-Aubert L, Carter SF, Almkvist O, Farid K, Scholl M et al (2016) Diverging longitudinal changes in astrocytosis and amyloid PET in autosomal dominant Alzheimer's disease. *Brain* 139:922–936
  31. Rusjan PM, Wilson AA, Miller L, Fan I, Mizrahi R, Houle S et al (2014) Kinetic modeling of the monoamine oxidase B radioligand [ $^{11}\text{C}$ ]SL25.1188 in human brain with high-resolution positron emission tomography. *J Cereb Blood Flow Metab* 34:883–889
  32. Saba W, Valette H, Peyronneau MA, Bramouille Y, Coulon C, Curet O et al (2010) [ $^{11}\text{C}$ ]SL25.1188, a new reversible radioligand to study the monoamine oxidase type B with PET: preclinical characterisation in nonhuman primate. *Synapse* 64:61–69
  33. Sander K, Lashley T, Gami P, Gendron T, Lythgoe MF, Rohrer JD et al (2016) Characterization of tau positron emission tomography tracer [ $^{18}\text{F}$ ]AV-1451 binding to postmortem tissue in Alzheimer's disease, primary tauopathies, and other dementias. *Alzheimers Dement* 12:1116–1124
  34. Santillo AF, Gambini JP, Lannfelt L, Langstrom B, Ulla-Marja L, Kilander L et al (2011) In vivo imaging of astrocytosis in Alzheimer's disease: an  $^{11}\text{C}$ -L-deuteriodoprenyl and PIB PET study. *Eur J Nucl Med Mol Imaging* 38:2202–2208
  35. Saura J, Luque JM, Cesura AM, Da Prada M, Chan-Palay V, Huber G et al (1994) Increased monoamine oxidase B activity in plaque-associated astrocytes of Alzheimer brains revealed by quantitative enzyme radioautography. *Neuroscience* 62:15–30
  36. Scholl M, Carter SF, Westman E, Rodriguez-Vieitez E, Almkvist O, Thordardottir S (2015) Early astrocytosis in autosomal dominant Alzheimer's disease measured in vivo by multi-tracer positron emission tomography. *Sci Rep* 5:16404
  37. Smith R, Puschmann A, Scholl M, Ohlsson T, van Swieten J, Honer M et al (2016) [ $^{18}\text{F}$ ]AV-1451 tau PET imaging correlates strongly with tau neuropathology in MAPT mutation carriers. *Brain* 139:2372–2379
  38. Smith R, Scholl M, Honer M, Nilsson CF, Englund E, Hansson O (2017) Tau neuropathology correlates with FDG-PET, but not AV-1451-PET, in progressive supranuclear palsy. *Acta Neuropathol* 133:149–151
  39. Taniguchi-Watanabe S, Arai T, Kametani F, Nonaka T, Masuda-Suzukake M, Tarutani A et al (2016) Biochemical classification of tauopathies by immunoblot, protein sequence and mass spectrometric analyses of sarkosyl-insoluble and trypsin-resistant tau. *Acta Neuropathol* 131:267–280
  40. Togo T, Dickson DW (2012) Tau accumulation in astrocytes in progressive supranuclear palsy is a degenerative rather than a reactive process. *Acta Neuropathol* 104:398–402
  41. Tong J, Rathitharan G, Meyer JH, Furukawa Y, Ang LC, Boileau I et al (2017) Brain monoamine oxidase B and a in human parkinsonian dopamine deficiency disorders. *Brain* 140:2460–2474
  42. Vermeiren C, Motte P, Viot D, Mairet-Coello G, Courade JP, Citron M et al (2018) The tau positron-emission tomography tracer AV-1451 binds with similar affinities to tau fibrils and monoamine oxidases. *Mov Disord* 33:273–281
  43. Villemagne VL (2018) Selective tau imaging: der stand der dinge. *J Nucl Med* 59:175–176
  44. Villemagne VL, Dore V, Burnham SC, Masters CL, Rowe CC (2018) Imaging tau and amyloid-beta proteinopathies in Alzheimer disease and other conditions. *Nat Rev Neurol* 14:225
  45. Williams DR, Holton JL, Strand C, Pittman A, de Silva R, Lees AJ et al (2007) Pathological tau burden and distribution distinguishes progressive supranuclear palsy-parkinsonism from Richardson's syndrome. *Brain* 130:1566–1576
  46. Xia CF, Artega J, Chen G, Gangadharmath U, Gomez LF, Kasi D et al (2013) [ $^{18}\text{F}$ ]T807, a novel tau positron emission tomography imaging agent for Alzheimer's disease. *Alzheimers Dement* 9:666–676